The Complementary Value of XBT and Argo Observations to Monitor Ocean Boundary Currents and Meridional Heat and Volume Transports: A Case Study in the Atlantic Ocean

MARLOS GOES,[a,b] GUSTAVO GONI,[b] SHENFU DONG,[b] TIMOTHY BOYER,[c] AND MOLLY BARINGER[b]

[a] *Cooperative Institute for Marine and Atmospheric Studies, University of Miami, Miami, Florida*
[b] *National Oceanic and Atmospheric Administration/Atlantic Oceanographic and Meteorological Laboratory, Miami, Florida*
[c] *National Oceanic and Atmospheric Administration/National Center for Environmental Information, College Park, Maryland*

(Manuscript received 19 February 2020, in final form 25 September 2020)

ABSTRACT: This work assesses the value of expendable bathythermograph (XBT) and Argo profiling float observations to monitor the Atlantic Ocean boundary current systems (BCS), meridional overturning circulation (MOC), and meridional heat transport (MHT). Data from six XBT transects and available Argo floats in the Atlantic Ocean for the period from 2000 to 2018 are used to estimate the structure and variability of the BCS, MOC, and MHT, taking into account different temporal and spatial mapping strategies. The comparison of Argo data density along these six XBT transects shows that Argo observations outnumber XBT observations only above mapping scales of 30 days and 3° boxes. The comparison of Argo and XBT data for the Brazil Current and Gulf Stream shows that Argo cannot reproduce the structure and variability of these currents, as it lacks sufficient resolution to resolve the gradients across these narrow jets. For the MHT and MOC, Argo estimates are similar to those produced by XBTs at a coarse mapping resolution of 5° and 30 days. However, at such a coarse resolution the root-mean-square errors calculated for both XBT and Argo estimates relative to a high-resolution baseline are higher than 3 Sv ($1\ \text{Sv} \equiv 10^6\ \text{m}^3\ \text{s}^{-1}$) and 0.25 PW for the MOC and MHT, respectively, accounting for about 25%–30% of their mean values due to the smoothing of eddy variability along the transects. A key result of this study is that using Argo and XBT data jointly, rather than separately, improves the estimates of MHT, MOC, and BCS.

KEYWORDS: Boundary currents; Mass fluxes/transport; In situ oceanic observations; Sampling; Error analysis; Oceanic variability

1. Introduction

Several efforts are currently under way to evaluate ocean observing platforms using a suite of data assimilation techniques, numerical models, and data impact studies (e.g., Vidard et al. 2007; Fujii et al. 2019). Although a level of data redundancy is often required to evaluate biases in the ocean observing system (Lyman et al. 2006; Cheng et al. 2014), each observing platform has unique capabilities with different strengths to address important observing system requirements. From 1970 to 2000, expendable bathythermograph (XBT) data accounted for approximately 40% of all temperature profile measurements used globally to monitor and evaluate the upper (<800 m) ocean state (Cheng et al. 2016). The global Argo profiling float program began in 1999, with each float providing profiles of temperature and salinity to a depth of 2000 dbar every 10 days. By 2004, the Argo array had become the main source of large-scale open ocean temperature and salinity measurements (Riser et al. 2016). Since the advent of Argo, the XBT sampling strategy has changed significantly, focusing mostly on repeat, across-basin transects designed to resolve mesoscale features (Goni et al. 2010). Although currently providing fewer observations, the global XBT network still accounts for approximately 5%–10% of all annual ocean temperature profiles (Goni et al. 2019). Unlike Argo floats that drift with the currents at 1000-m nominal parking depth, XBTs repeatedly monitor the variability of ocean currents (i.e., boundary currents and surface/subsurface currents) and basinwide integrated heat and volume transports across fixed high-density sections. XBT transect observations also have the advantage of being relatively low cost, with deployments generally coming from commercial vessels.

Boundary currents carry a significant part of the transport of mass and heat in the ocean (Sutton and Allen 1997; Visbeck et al. 2003; Todd et al. 2019) and, therefore, are a key component of the transbasin meridional volume and heat transport (MHT). Long-term variations of MHT have been shown to modulate regional and global weather patterns (Lopez et al. 2016), as well as large-scale upper ocean heat content and steric sea level (e.g., Woodworth et al. 2014; Volkov et al. 2019), which may cause different impacts on boundary currents and coastal sea level (Domingues et al. 2018). Sustained observations are paramount for monitoring long-term variability (interannual to decadal) and secular trends of ocean currents. Some of the longest records (>50 years) of the structure, and volume and heat transports of ocean currents are available using along-transect XBT data (Goni et al. 2019). The value of integrating XBT data with data from other observational platforms, particularly Argo profiling floats and satellite altimetry, has been recognized by the scientific community as an effective way to reduce data gaps, extend coverage, and improve sampling at different temporal and spatial scales around the globe. For instance, this data integration has been used to

Supplemental information related to this paper is available at the Journals Online website: https://doi.org/10.1175/JTECH-D-20-0027.s1.

Corresponding author: Marlos Goes, marlos.goes@noaa.gov

DOI: 10.1175/JTECH-D-20-0027.1

investigate the East Australian Current (Ridgway et al. 2008; Rykova and Oke 2015; Zilberman et al. 2018), Indonesian Throughflow (Wijffels and Meyers 2004), Gulf Stream (Andres 2016; Dong et al. 2019), Brazil Current (Goes et al. 2019; Majumder et al. 2019), Atlantic off-equatorial currents (Goni and Baringer 2002; Goes et al. 2013), Antarctic Circumpolar Current fronts (Swart et al. 2008; Domingues et al. 2014), and transbasin integrated meridional overturning circulation (MOC) and MHT (Douglass et al. 2010; Dong et al. 2015). The complementarity between XBT and Argo observations has also been extensively explored for estimates of ocean heat content and steric sea level (e.g., Cheng et al. 2017; Dieng et al. 2017). For this purpose, several global gridded observational products using Argo and XBT data are available, which differ mostly on mapping procedures, baseline climatology, and bias corrections (e.g., Boyer et al. 2016).

Given the contributions of the XBT and Argo observational platforms for monitoring and understanding ocean circulation, and their potential complementarity in measuring boundary current systems (BCS), MOC, and MHT, it is important to evaluate whether observations from Argo can fully reproduce the results obtained from using the older XBT technology under their current sampling strategies. It is also important to determine whether a combination of the two can improve time series estimate indices. Studies such as ours can also help to assess the gaps and synergies of other technologies and sampling strategies in the global observing system (e.g., gliders, drifters, and moorings).

Numerical modeling studies have been used to evaluate the sampling strategies of XBT and Argo data. For example, Vecchi and Harrison (2007) simulated how Argo and XBT reproduce ocean variability in the Indian Ocean. They found that while Argo floats captured the large-scale intraseasonal to interannual variability, XBTs provided better sampling and less uncertainty in key regions, particularly across boundary currents, upwelling, and equatorial areas where Argo sampling is generally sparse. Dong et al. (2011) showed that despite the lack of Argo data at the boundaries, Argo data assimilation is beneficial by strengthening the boundary currents in an ocean model, probably due to better temperature/salinity representation at the interior side of the boundaries. Indeed, observing system experiments show that Argo has a broad impact on model assimilation, whereas the effect of assimilating ship-based profiles is more localized along-transects (Zuo et al. 2019). In another study, Goes et al. (2015) evaluated the temporal and spatial sampling of XBTs to monitor the MOC in the South Atlantic Ocean at 34.5°S. They showed that a minimum of 15 years of quarterly sampling was necessary for the seasonal cycle of transport to converge, and that sampling at the boundaries needed to be measured at eddy-permitting spatial resolution.

The goal of this work is to assess how Argo and XBT data capture the variability of the BCS, MHT, and MOC and to investigate the value of combining Argo and XBT data using their current observational strategies. The analysis presented here focuses on Argo and XBT data collected around six XBT transects in the Atlantic Ocean, although results and conclusions may also apply to other basins and ocean current systems.

This manuscript is outlined as follows. Section 2 presents the XBT and Argo datasets and main methods used to estimate the BCS, MOC, and MHT from the data. Section 3 provides an analysis of the four main objectives of this study: 1) assess the availability/density of Argo data along XBT transects to discern which spatial and temporal scales can be identified from Argo data to monitor BCS and MHT; 2) assess the sampling trade-offs between the XBT and Argo observing systems, comparing the advantages of the spatial cohesion of the data versus the more frequent temporal coverage of Argo floats; 3) compare boundary currents and meridional heat and volume transports derived from XBT and Argo data; and 4) test the implementation of an integrated observing system for MHT monitoring using both Argo and XBT observations. In section 4, we discuss the benefits of using Argo and XBT data and their integrability and complementarity with other components of the ocean observing system to better monitor MHT and boundary currents.

2. Data and methods

a. Data

We used data from six high density XBT transects (ranging from 10- to 35-km sampling resolution) and Argo profiling floats in the Atlantic Ocean (Fig. 1). These transects are important for monitoring BCS including the Gulf Stream (XBT transects AX07, AX10, AX32; and AX08, which is not analyzed here) and the Brazil Current (AX97, AX18), the Antarctic Circumpolar Current fronts (AX25; and AX22 in the Drake Passage, which is not analyzed here), and for monitoring the MOC and MHT with two cross-basin zonal transects at approximately 34.5°S (AX18) and 27°N (AX07). The average temporal sampling of these transects is every 3 months (i.e., quarterly), with two transects deployed at a higher temporal sampling rate (AX32 is deployed monthly, and AX97 is deployed every 2 months), and one transect deployed at a lower temporal sampling rate, i.e., AX25, which is sampled twice a year and mostly during summer months due to weather conditions in the Southern Ocean. Consequently, AX25 has the lowest number of realizations, only 36, while AX32 has the most with 409 realizations. XBT temperature profile data in the upper 800 m are from the NOAA/AOML database (http://www.aoml.noaa.gov/phod/hdenxbt/). Only profiles that were flagged as good following quality control procedures were considered. Salinity profiles from XBT deployments were derived using the regression method of Goes et al. (2018). To complete the profiles for the full water column, a 0.25° resolution of the seasonal climatology of temperature and salinity (T–S) profiles from the *World Ocean Atlas 2013* (*WOA13*) (Locarnini et al. 2013; Zweng et al. 2013) was used below 800 m. Each T–S profile was linearly interpolated to 140 standard depths, starting from 5 m at 10-m intervals until 750 m, 50-m intervals until 2000 m, and 100-m intervals until a maximum of 6000 m. We also used delayed mode Argo profile data from the Global Argo Data Repository of the National Centers for Environmental Information (https://www.nodc.noaa.gov/argo/) for T–S profiles flagged as good or as potentially good (flags 1, 2, 5, 8 from http://www.argodatamgt.org/Documentation). Similar to the

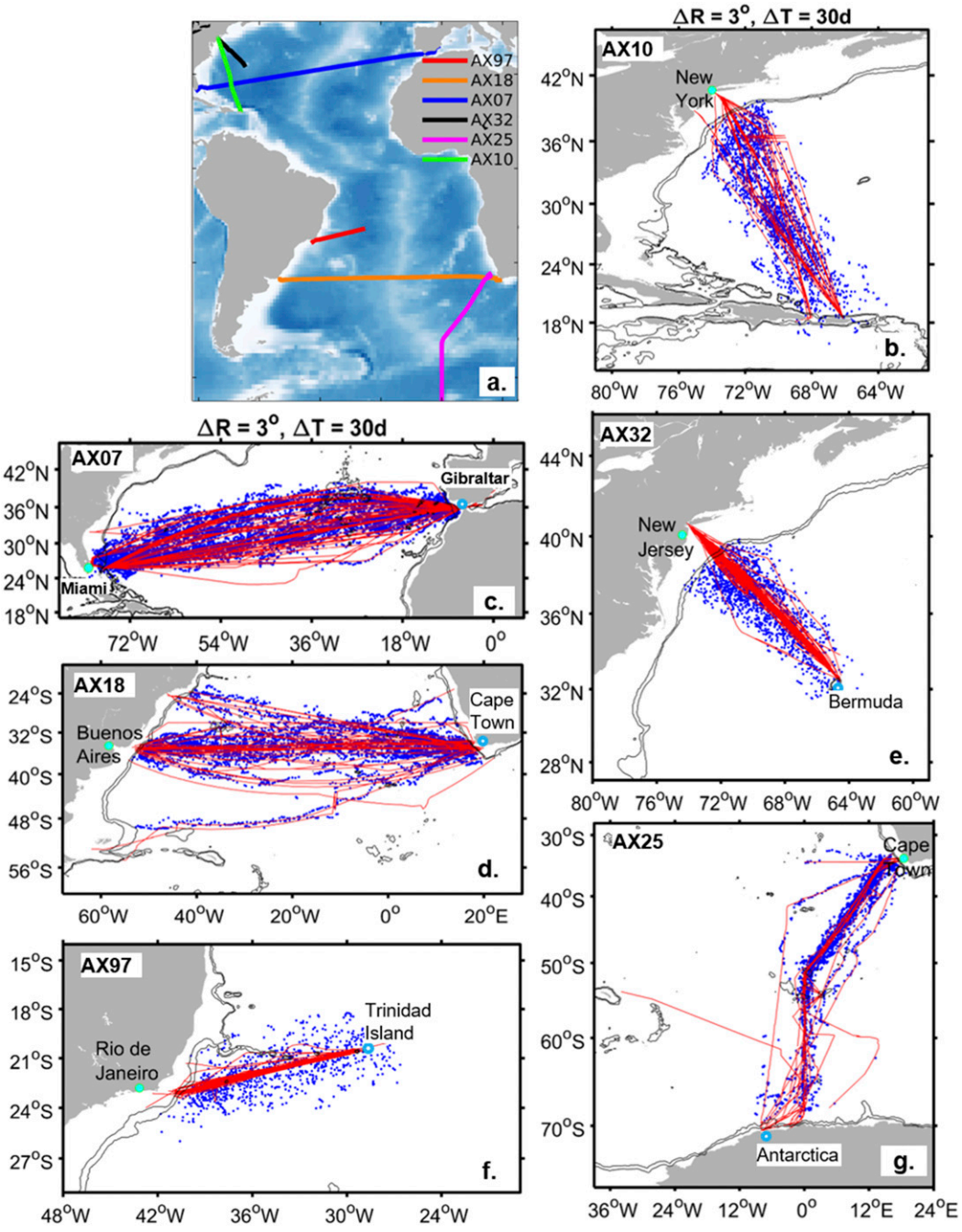

FIG. 1. Data analyzed along the six XBT transects considered: (a) Locations of the nominal XBT transects (colored lines). Shown are zonal transects (c) AX07, (d) AX18, and (f) AX97 and meridional transects (b) AX10, (e) AX32, and (g) AX25. Red dots are the XBT deployments, and blue dots are the Argo profiles within $\Delta T = 30$ days and 3° of each XBT profile.

XBT data, the Argo *T*–*S* profile data were also interpolated to standard depths and padded to the bottom of the ocean using the *WOA13* climatology. The disparity found in some profiles in which the available salinity data were fewer than the temperature data was circumvented by applying the same regression methodology to estimate salinity for the XBT profiles. Differently from XBT profiles, the padding of Argo profiles was only applied below 1600 m to take advantage of the deeper coverage of the Argo data, since many of the Argo profiles had available data down to 1500 or 2000 m. Sensitivity tests performed with Argo data showed that the effect of padding from 800 to 1600 m was negligible relative to

TABLE 1. Main sampling characteristics and estimated physical parameters of the six XBT transects analyzed in this study. For the parameter, BC = Brazil Current, MOC = meridional overturning circulation, MHT = meridional heat transport, ACC = Antarctic Circumpolar Current, AC = Agulhas Current, and GS = Gulf Stream; ΔT_0 is the mean duration of the transect in days.

	AX97	AX18	AX25	AX07	AX32	AX10
Parameter	BC	MOC/MHT, BC	ACC, AC	MOC/MHT, GS	GS	GS
Initial year	2004	2000	2004	1995	1977	1997
Duration (ΔT_0)	5	9	8	11	2	5
Direction	Zonal	Zonal	Meridional	Zonal	Meridional	Meridional
Profiles per transect	50	300	100	270	45	100
Realizations until 2018	62	50	36	93	409	80
Argo lon range	60°–20°W	70°W–20°E	20°W–20°E	82°–6°W	82°–30°W	82°–40°W
Argo lat range	15°–30°S	20°–50°S	32°–70°S	40°–20°N	50°–20°N	50°N–0°
No. of Argo profiles	13 782	101 888	50 546	99 615	94 309	80 735

uncertainties that arise from the sampling strategies and from the methods of heat and volume transports calculation. For the analysis, a subgroup of the Argo data population was provided for the location of each transect using a broad latitudinal and longitudinal range, as shown in Table 1, with all data considered until December 2018.

b. Method

1) ALONG-TRANSECT MAPPING DEFINITION

To compare Argo and XBT samplings near the six analyzed XBT transects, we first calculated the number of XBT and Argo profiles in the vicinity of each XBT deployment, and then examined profile data densities along each transect. The total number of transect realizations and the average number of XBT deployments along each transect are given in Table 1. The number of Argo profiles in the vicinity of an XBT deployment, as well as the mapping of T–S profiles along a transect, was determined by searching all profiles within defined space–time boundaries centered on the particular deployment. To accomplish this, we used two parameters: 1) ΔR, defined as the radius of a circular search area in space (in degrees of latitude/longitude); and 2) ΔT, the length of the search period in days added to the time span to complete a corresponding XBT transect (ΔT_0). The resulting search period varies slightly for each transect, as given by the average ΔT_0 values in Table 1. We allowed the search period to vary from $\Delta T = 2.5$ days to $\Delta T = 90$ days, which is under the period for repeating a quarterly XBT transect, and the search area radius to vary from $\Delta R = 0.25°$ to $\Delta R = 5°$.

The T–S mapping along the transect consisted in weighted averages of the nearby profiles using a normalized separable exponential function in time and space (Goes et al. 2010), given by

$$W = \exp\left(\frac{\sqrt{x^2 + y^2}}{\Delta R}\right) \times \exp\left(\frac{\sqrt{T^2}}{\Delta T}\right). \quad (1)$$

Because of the spatial variability of the XBT transect realizations, global statistics for each transect are presented along a nominal transect (Fig. 1a). Each nominal XBT transect was calculated by first interpolating every realization to a standardized distance given as the median distance between deployments (~25 km). The results are presented along the main direction of the transect, defined as either "meridional" or "zonal," depending on the maximum range in each direction. Following this definition, AX97, AX18, AX07 were treated as zonal transects, and AX25, AX32, and AX10 were considered meridional transects (Fig. 1 and Table 1).

2) BOUNDARY CURRENTS AND MERIDIONAL HEAT AND VOLUME TRANSPORT

To investigate the sensitivity of the ocean property estimates to the XBT and Argo samplings along the analyzed XBT transects, we remapped the sections with various spatial and temporal resolutions from XBT and Argo measurements using the method described in section 2b(1). We then compared the integrated MHT, and the absolute geostrophic velocity and volume transport of the boundary currents derived from these sections. The time-mean transport values are calculated as their sample mean, and their 95% confidence interval (CI) are estimated as 1.96 standard errors from the sample mean. The geostrophic velocities of the BCS were estimated using the thermal wind relationship relative to a level of known motion (e.g., Goes et al. 2019), where a gridded monthly climatology of absolute dynamic topography on standard levels is derived from the International Pacific Research Center gridded merged altimetry and Argo product (e.g., Yu et al. 2006). For the two BCS we studied, the climatological reference dynamical topography was defined at 500 m for the Brazil Current, which is the approximate location of the boundary between Central and Intermediate Waters (Boebel et al. 1999), and 1000 m for the Gulf Stream. In addition, velocities are extrapolated to the shelf from the last mapped profiles.

The integrated MHT and MOC in the South Atlantic are composed of Ekman and geostrophic contributions (Dong et al. 2009; Goes et al. 2015). For the North Atlantic near 27°N, where the Florida Strait is located, we used measurements of the Florida Current transport to close the meridional mass budget (McCarthy et al. 2015), with monthly transport averages derived from flow-induced voltage measurements from a submarine telephone cable between Florida and the Bahamas (http://www.aoml.noaa.gov/phod/floridacurrent/). As an approximation, the gridded velocity field across the Florida Strait (west of 78°W) was calculated by equally distributing the Florida Current transport across the area of the Florida Strait.

We linearly interpolated the data along the transect and used *T*–*S* profiles from the *WOA13* to complete the entire section from the western to eastern boundaries for MHT and MOC calculations. These profiles are averaged to the same resolution used in the data mapping to keep consistency. The extrapolation with climatological profiles was particularly important for the Argo estimates to fill gaps in the Florida Strait and near the eastern boundary.

The Ekman component was calculated using the ERA-Interim monthly wind stress dataset (Dee et al. 2011). The meridional and zonal components of the wind stress were interpolated for the month, mapped for locations along the transect, and projected to the direction of the transect. The methodology to calculate the cross transect velocities needed to generate the MHT and MOC streamfunction is explained in Baehr et al. (2004) and Goes et al. (2015). Here, the reference for the geostrophic velocity calculation comes from the Argo's YoMaHa'07 product (Lebedev et al. 2007), which provides gridded annual climatological mean derived from Argo float displacements at a nominal depth of 1000 m. In addition, a mass balance is applied to each sampled section to estimate the MOC streamfunction, and the MOC strength is then calculated as the maximum absolute value of the streamfunction.

3. Results

a. Density of Argo data along XBT transects

An example of data selection near an XBT transect is shown in Fig. 1. The XBT measurements show some spatial variability relative to their nominal transect due to changes in ship routes. Most of this variability is constrained within 5° of the nominal transect with a few exceptions, such as the AX18 transect (Fig. 1d), which exhibits stronger changes over time near its western boundary. Argo profile data distributed near the XBT measurements sampled within 30 days and a 3° radius show that Argo data consistently sampled all regions of the XBT transects. The histograms of data distribution along each XBT transect are presented in Fig. 2 for various mapping resolutions. There is a general agreement among the histograms of different transects. At higher spatial resolution ($\Delta R = 0.25°$; $\Delta R = 0.5°$), Argo data are almost nonexistent along the transects, with an average of 0.2 Argo profiles per radius. This indicates that the Argo data, which are more evenly spread in space, cannot resolve the same spatial mesoscale variability targeted by the XBT transects in specific regions. When the high spatial sampling strategy is relaxed (Fig. 2, right column), the number of Argo profiles increases relative to XBT profiles. This is because the search area for Argo profiles increases quadratically with the search radius, whereas the number of along-transect XBT profiles increases linearly with an increased area radius. However, for the low-spatial-resolution parameter settings ($\Delta T = 30$ days; $\Delta R = 1°$ or 3°), XBT data still present a higher density than Argo along the XBT transects. This difference is amplified near the boundaries, where most XBT transects have increased sampling, which is critical for resolving boundary currents. For the AX32 transect (Fig. 2b), Argo surpasses XBT sampling in the offshore location of this transect (south of 36°N). This is explained by the shorter range of the transect earlier in the analyzed period, as this transect spanned from New Jersey to ~37°N to measure the shelf and slope region north of the Gulf Stream, and in the late 2000s it was extended to Bermuda (Fig. 1e). In addition, because of its operational design, Argo float observations are usually restricted to regions with depths greater than 2000 m, whereas boundary current regions include shallower depths.

b. Sampling trade-offs between current XBT and Argo observations

As shown in section 3a, Argo data are more evenly distributed in a two-dimensional space (increases proportional to ΔR^2), whereas the XBT sampling is mostly linear in space (increases proportional to ΔR). Therefore, the density of Argo profiles is expected to exceed the density of XBT data for larger values of time (ΔT) and space (ΔR) mapping. We define sampling trade-offs as the boundary in the mapping parameter space, above which the Argo sampling rate exceeds XBT sampling rate. For this, the median number of along-transect profiles was calculated separately for Argo and XBT observations in areas defined by different spatial and temporal sizes (Fig. S1 in the online supplemental material). These values are averaged over time, counting only the transect realizations with available data. Therefore, the mean values produced for each mapping parameter set are fairly independent of the number of realizations or the beginning time of the transect (Table 1).

A comparison between the current XBT and Argo sampling strategies is summarized in a two-dimensional diagram showing the average difference (XBT − Argo) in the number of profiles within the space (*x* axis) and time (*y* axis) mapping resolution along each XBT transect (Fig. 3). The red shades in Fig. 3 show that in all transects the XBT data outnumber the Argo data for nearly all of the mapping parameter space sampled. The XBT sampling strategy improves upon the Argo strategy in regions of high spatial and temporal sampling, mostly along the horizontal (spatial) axis, since the maximum time sampling of 90 days is generally below the average quarterly repetition of a single XBT transect. The sampling trade-off is shown as the black contour line in Fig. 3. In general, Argo profiles outnumber XBT profiles for sampling $\Delta R > 3°$ and $\Delta T > 30$ days. The number of Argo float observations along the AX10 and AX97 transects only surpassed XBT sampling in a very narrow region of the analyzed range of mapping parameters ($\Delta T = 90$ days; $\Delta T = 5°$ mapping). The AX32 transect, like AX10, also measures the Gulf Stream but shows a better trade-off for Argo when compared with AX10 ($\Delta T = 20$ days; $\Delta R = 5°$) which, as shown in Fig. 2b, is due to lower historical sampling in its offshore location. The AX25 transect, with the least number of realizations, does not differ significantly from the other transects. Therefore, these results show that Argo sampling generally exceeds XBT sampling at mapping resolutions coarser than 3° and 30 days. Although not previously quantified, this result is expected since this is the nominal resolution for Argo floats.

c. Boundary currents constrained by Argo float data along XBT transects

We present two examples of boundary currents that are observed by XBT transects: (i) the Brazil Current measured

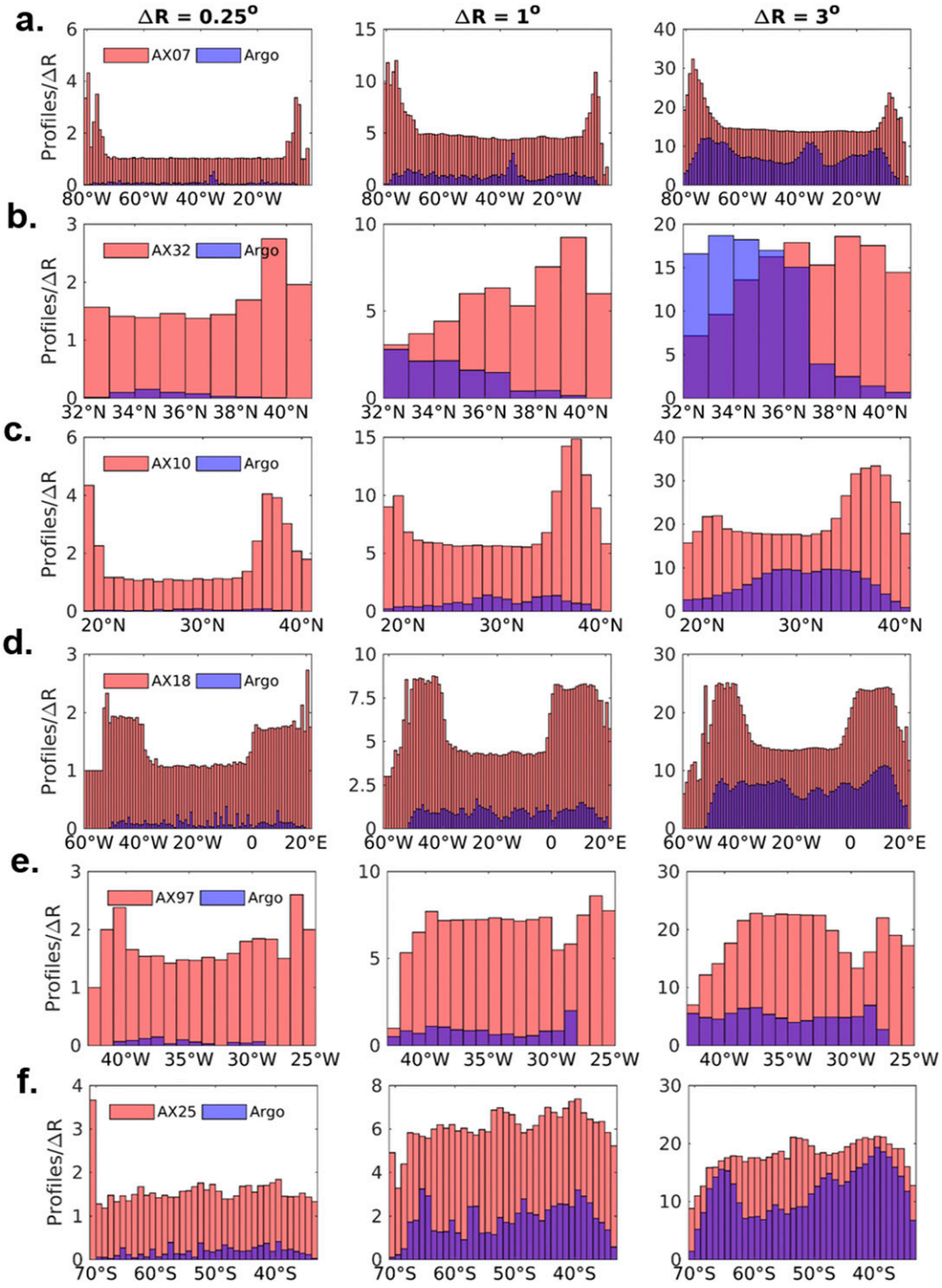

FIG. 2. Histograms of the mean number of XBT (red) and Argo (blue) profiles per mapped radius (ΔR; °) obtained along each XBT transect, taking into account all data within $\Delta T = 30$ days of the transect. Each row is for one transect: (a) AX07, (b) AX32, (c) AX10, (d) AX18, (e) AX97, and (f) AX25. The columns represent each box radius of (left) $\Delta R = 0.25°$, (center) $\Delta R = 1°$, and (right) $\Delta R = 3°$. Bars are shown at 1° classes following the main direction of the transect.

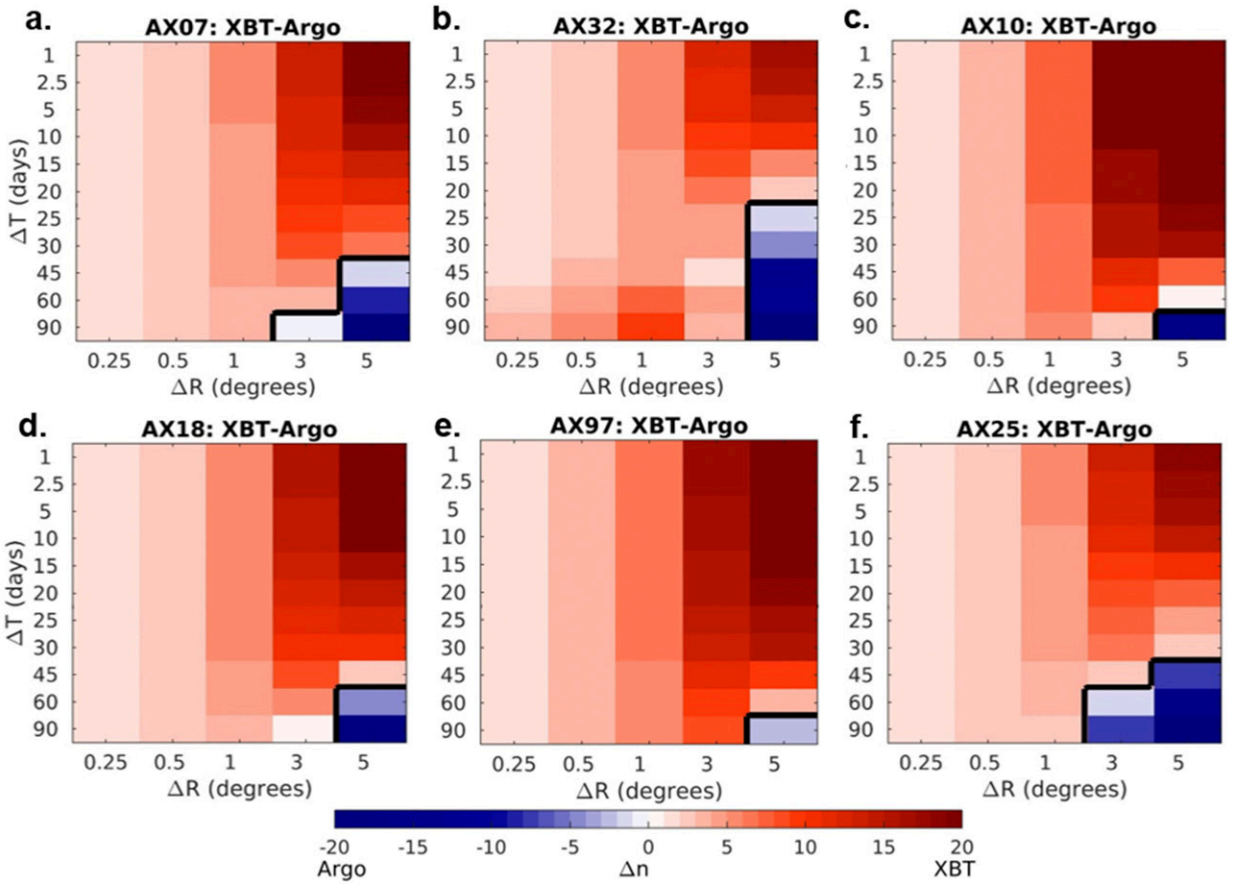

FIG. 3. Sampling difference between Argo and XBT data for each XBT transect. The filled contours represent the difference in the number of observations (XBT − Argo) along each transect, accounting for the different time (y axis) and distance (x axis) sampling box averages. The black line represents the trade-off limit, above which the Argo sampling rate (blue shades) exceeds the XBT sampling rate (red shades).

using XBT observations from the AX97 transect located at approximately 22°S and (ii) the Gulf Stream measured by AX10 XBT transect observations between 35° and 40°N. These results can be extended to eastern boundary currents (e.g., the Benguela Current using the AX18 transect) and ACC fronts (using AX25; see Fig. S2 and Text S2 in the online supplemental material for a brief analysis), which were not analyzed.

1) BRAZIL CURRENT

The Brazil Current near 22°S is a southward flowing narrow jet extending from the shelf until approximately 39°W, with a mean core velocity of around 25 cm s^{-1} extending from the surface to 500-m depth (Goes et al. 2019). Below the Brazil Current, the intermediate western boundary current (da Silveira et al. 2004) is observed flowing northward, showing the strong baroclinicity of the region. The differences in the time mean geostrophic velocity derived from Argo and XBT arise mostly near the coast (Fig. 4). Argo floats cannot sample the continental slope located west of 40°W. On the other hand, XBT observations reach as far as 42°W and can retrieve temperature information across the shelf. This difference results in a distinct representation of the Brazil Current. XBT data resolve the full extension of the Brazil Current, which is generally located west of 39°W, at a resolution better than 1° sampling. As the resolution decreases, the Brazil Current becomes wider and more diffuse. As larger horizontal boxes are used and the information is degraded, the data lose their representativeness near the shelf. At 3° sampling, the Brazil Current practically disappears (Fig. 4d). For the Argo data, the Brazil Current cannot be resolved at either 1° or 3° sampling. At 0.25° and 0.5° sampling, the derived Brazil Current reverses direction, showing a mean northward flow instead of southward, and the transport values are not significantly different from zero. This reversal of the Brazil Current by Argo estimates can be explained by the lack of observations near the shore. The characteristic trough in the dynamic height field from a western boundary current (see Fig. 2 in Goes et al. 2019) is missed by Argo, and it is instead represented by the crest in the dynamic height from the outbound limit of the Brazil Current (~39°W). The transport of the Brazil Current near 22°S is calculated integrating the southward velocities from the surface to 500 m, and zonally from the coast to 38°W. Using the XBT data at a 0.25° mapping resolution, the derived mean Brazil Current

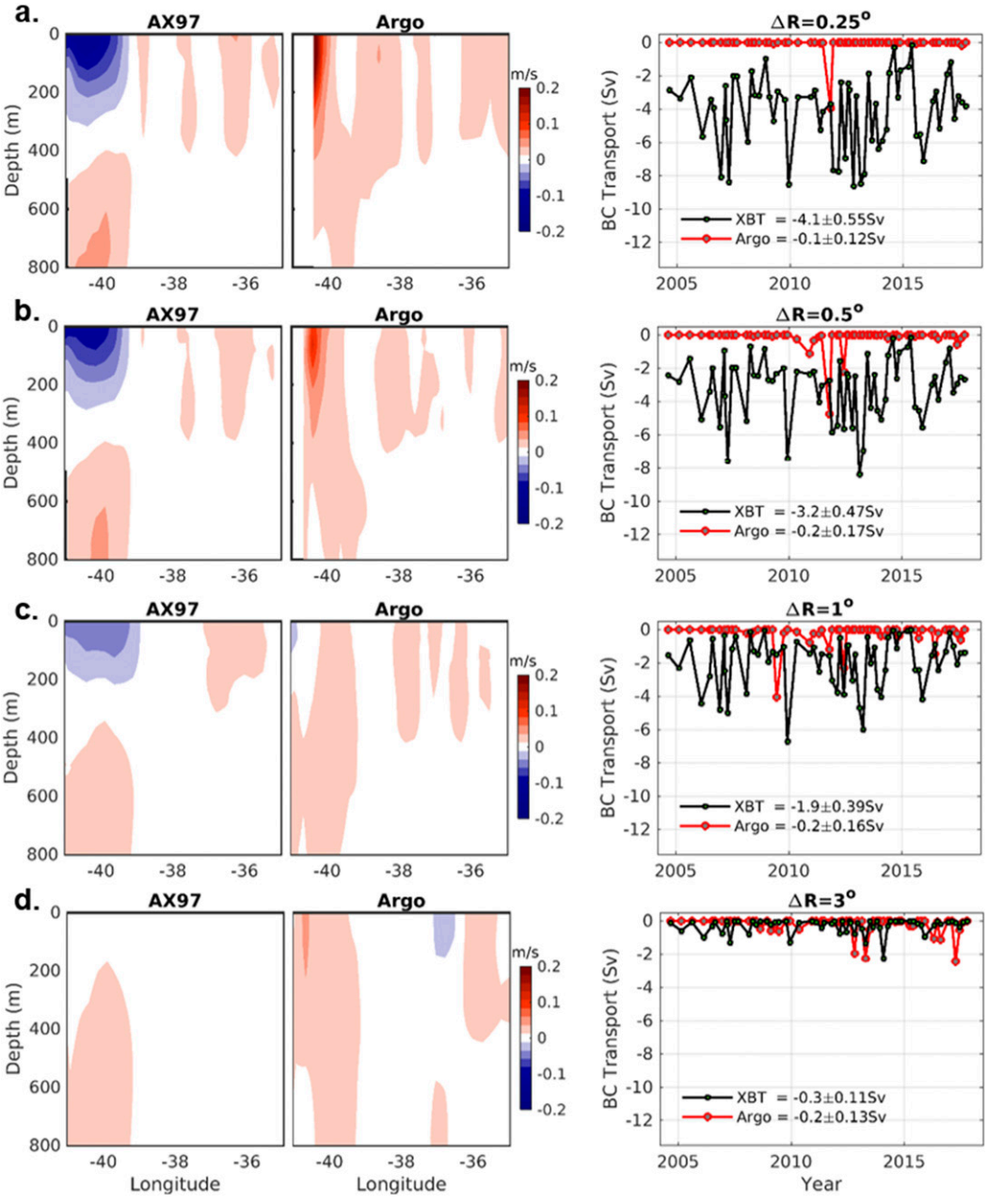

FIG. 4. Brazil Current time-mean geostrophic velocity sections near 22°S (Fig. 1a) as measured by the (left) AX97 XBT transect and (center) Argo using different spatial boxes of ΔR of (a) 0.25°, (b) 0.5°, (c) 1°, and (d) 3° and ΔT = 30 days. (right) The Brazil Current transport time series (Sv) derived from XBT (black) and Argo (red) along the XBT transect; the values shown are their respective time mean and 95% CI.

transport is 4.1 ± 0.5 Sv (1 Sv = 10^6 m^3 s^{-1}), which is within the range of previous observational estimates from altimetry and hydrography data near 22°S (e.g., Goes et al. 2019). At 0.5°, the variability is still comparable but with a slightly weaker flow of 3.2 ± 0.5 Sv. At 1° mapping resolution, the mean transport decreases by 50%. Because the Brazil Current is a weak and narrow western boundary current, at lower resolution its volume transport practically disappears. Argo cannot resolve the Brazil Current transport in any circumstance of the mapping parameter space. These estimates are not particularly sensitive to different temporal mappings analyzed.

2) GULF STREAM

Off Cape Hatteras (~75°W/35°N), the Gulf Stream transitions from a trapped western boundary current to a meandering free jet flowing northeastward (Andres 2016). The western boundary near 35°–40°N shows two distinct

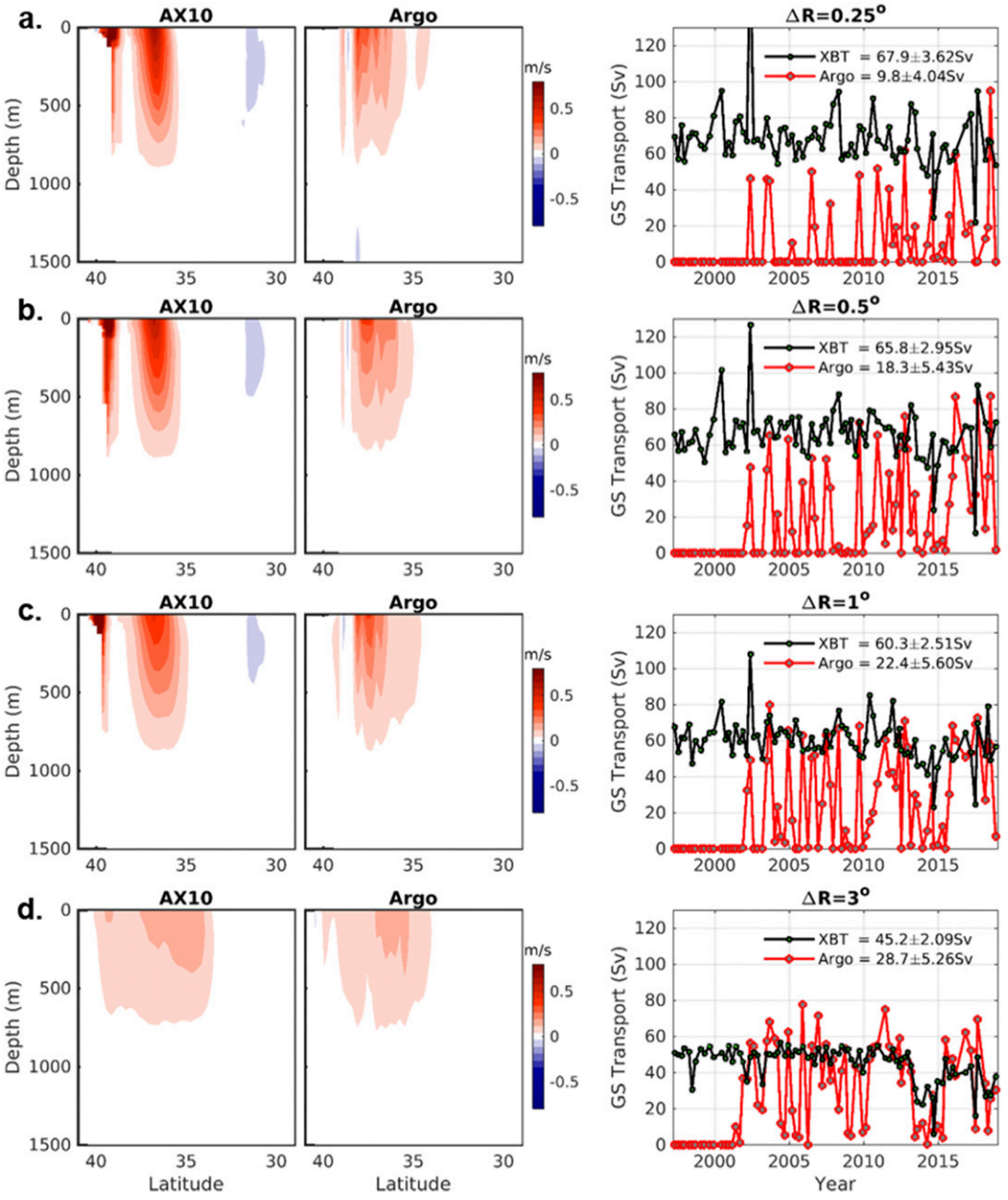

FIG. 5. Gulf Stream (GS) time-mean geostrophic velocity sections near 37°N (Fig. 1a) as measured by the (left) AX10 XBT transect and (center) Argo using different spatial boxes of ΔR of (a) 0.25°, (b) 0.5°, (c) 1°, and (d) 3° and $\Delta T = 30$ days. (right) The GS transport time series (Sv) derived from XBT (black) and Argo (red) along the XBT transect; the values shown are their respective time mean and 95% CI.

velocity cores, the Gulf Stream farther offshore and the shelfbreak jet, which is a narrow coastal jet flowing northward (Flagg et al. 2006). The AX10 XBT transect data distinguish the two strong jets with average core velocities of nearly 80 cm s^{-1} (Fig. 5a). As the spatial resolution decreases, the two cores merge into one single and weaker jet (Fig. 5d). The Gulf Stream transport near 39°N is calculated integrating the northward velocities from 0 to 800 m and from the coast to 33°N. Similar to the Brazil Current, the Gulf Stream transport is also stronger when the current is better resolved, and XBTs show a mean transport value of 67.9 ± 3.6 Sv at 0.25° sampling. This value decreases to 60.3 ± 2.5 Sv at 1° resolution when the two distinct cores are still observed and to ~45.2 ± 2.1 Sv at 3° resolution, a reduction of 30%. Using only Argo data, only a few realizations show more comparable values of transport of nearly 40 Sv at 0.25° (~62% of those from XBTs), but it misses most of the variability. Since the Gulf Stream at this latitude is mostly

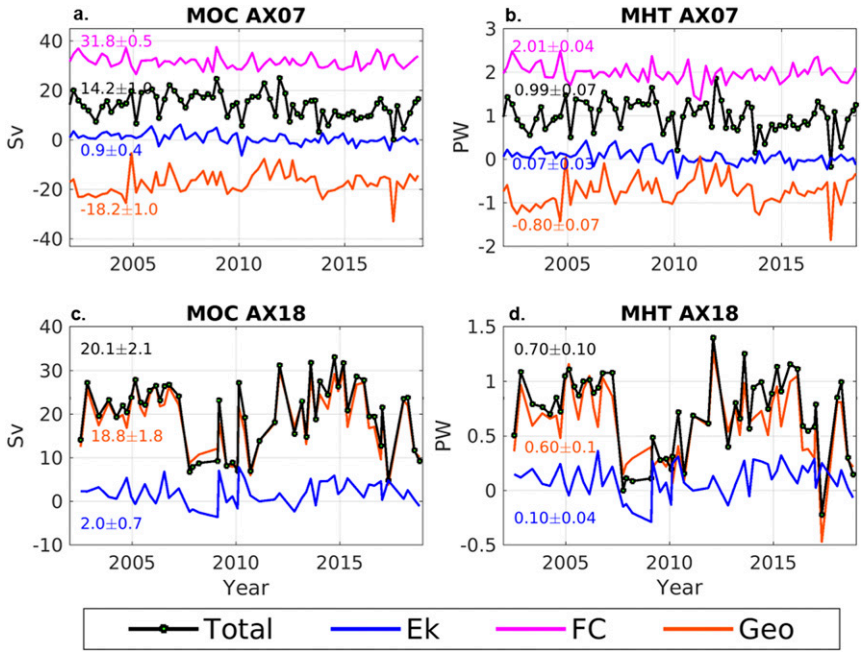

FIG. 6. Atlantic (left) MOC and (right) MHT components across the (a),(b) AX07 and (c),(d) AX18 transects as measured by XBT transect data (black lines) using spatial boxes of ΔR = 0.25° and ΔT = 30 days. The other lines are the components of the MHT and MOC [Ekman (Ek): blue; Florida Current (FC): magenta; geostrophic (Geo): orange]. The time mean and 95% CI are included in each panel.

located offshore, the temporal representativeness of its transport by Argo increases as the resolution decreases. Consequently, Argo data reach a higher mean transport value of ~28.7 ± 5.3 Sv at 3° sampling. Although the Argo-derived transport and core velocity values of the Gulf Stream are more comparable to those from XBTs using low resolution, they are about one-half of their XBT baseline values.

The results for the two boundary currents presented here show that the current sampling from Argo observations cannot resolve these narrow jets at higher spatial resolution, particularly the ones that flow close to the shelf break, and the derived transport values are subject to strong temporal variance due to uneven float coverage. At coarser resolutions, when Argo observations may exceed the XBT sampling (Fig. 3), these currents either disappear or produce about 65% lower volume transport values.

d. *Meridional heat and volume transport constrained by Argo float data along XBT transects*

In this section we compare the MHT and MOC estimates derived from XBTs and Argo at two locations, the South Atlantic at the nominal latitude of 35°S and the North Atlantic at the nominal latitude of 27°N, using data along the AX18 and AX07 transects, respectively. According to the method described in section 2b(2), the MOC along the AX07 transect includes three main contributions (Fig. 6a). The Florida Current is the strongest contributor, accounting for 31.8 ± 0.5 Sv northward. The Ekman transport is the smallest, with a mean contribution of 0.07 ± 0.03 Sv, which is 3 to 4 Sv lower than the estimates for 26.5°N (Johns et al. 2011; McCarthy et al. 2015). The third is a southward geostrophic contribution of 18.2 ± 1.0 Sv, which is similar to the upper midocean (UMO) transport calculated from the Rapid Climate Change Meridional Overturning Circulation Heat-Flux Array Western Boundary Time Series (RAPID-MOCHA-WBTS) mooring array along 26°N (McCarthy et al. 2015). UMO is southward because it contains contributions from the recirculation of thermocline waters, and also from the southward transport of the North Atlantic Deep Water (Bryden et al. 2005). The sum of these contributions produces a total transport of 14.2 ± 0.5 Sv of MOC, which are ~3 Sv smaller than the one estimated by the RAPID-MOCHA-WBTS array at 26°N, which is expected since the AX07 XBT transect is at an angle relative to that latitude, reaching the latitude of Gibraltar at its eastern boundary (Figs. 1a,c). The derived MHT for the North Atlantic included a northward transport of 2.01 ± 0.04 across the Florida Straits, a 0.07 ± 0.03 PW of Ekman transport, and a southward geostrophic contribution of 0.80 ± 0.07 PW. These MHT components are small relative to their respective means of 2.5, 0.35, and (−)1.77 PW along the 26°N section (Johns et al. 2011). The total MHT for the AX07 is 0.99 ± 0.07 PW, which is also small in comparison with the mean 1.35 PW from the RAPID-MOCHA-WBTS array at 26°N.

The MOC and MHT calculated from Argo observations (Fig. 7) generally ranges from 1 to 3 Sv and 0.05 to 0.2 PW lower than the XBT estimates, respectively, and much more variable. Using a ΔR = 3° mapping (Fig. 7, bottom panels) results in a more complete coverage of the basin and shows a similar mean

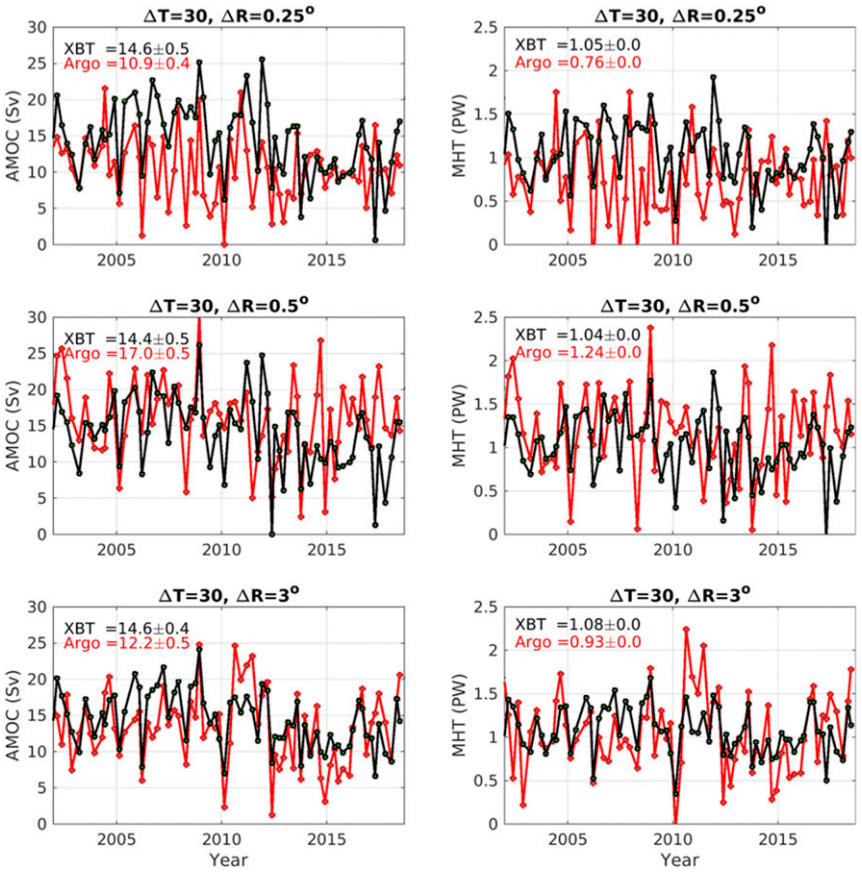

FIG. 7. Time series of the (left) North Atlantic MOC and (right) MHT estimated along the AX07 transect (see Fig. 1a) for Argo (red) and XBT (black) data for a ΔT = 30-day time mapping and spatial mapping resolution of ΔR for (top) 0.25°, (middle) 0.5°, and (bottom) 3°. The time mean and 95% CI are included in each panel.

value to the value calculated from XBT observations, although Argo-derived MOC variability is still much stronger. This high variability is due to the geostrophic transport (not shown), driven mostly by the large spatial gaps found along the section for Argo, even when applying a 3° mapping, and maybe also from vertical gaps, which are interpolated in the profiles.

In the South Atlantic at 35°S, the MOC and MHT measured by the AX18 transect includes two main components, Ekman and geostrophic (Fig. 6b). The mean Ekman transport is 2 ± 0.7 Sv and the mean geostrophic component is 18.8 ± 1.8 Sv, for a total 20.1 ± 2.1 Sv of MOC transport. The time-mean MHT is 0.7 ± 0.1 PW, and includes contributions of 0.1 ± 0.04 PW from Ekman and 0.6 ± 0.1 PW from geostrophic transports. These values are higher than the estimates of ~19 Sv and 0.59 PW from Dong et al. (2015), which is probably due to the different time span and methodology used to calculate the MOC. At 35°S, the MHT and MOC from Argo data follow the same long-term variability as XBT estimates (Fig. 8), shown by a weakening between 2006 and 2011 and later recovery, which is due to the variability in the location of the transect. Similar to estimates for the North Atlantic, the year-to-year variability in the South Atlantic is noisier based on Argo estimates, but the discrepancy increase related to the spatial resolution is less visible.

To quantify the discrepancy between the XBT and Argo estimates of MHT and MOC, we calculated the root-mean-square error (RMSE) of the time series relative to the XBT baseline, considered here as the estimates with $\Delta R = 0.25°$ for both AX07 and AX18. For this we used estimates at ΔT = 30-day averages, which improved the Argo sampling across the basin. Argo and XBT estimates show different relationships with respect to the spatial resolution (Fig. 9). For XBT data, decreasing the mapping resolution from 0.25° to 5° increased the RMSE of the MOC and MHT estimates almost linearly from 0 to 3.0 Sv and from 0 to 0.24 PW for the AX07 transect (Figs. 9a,b) and from 0 to 6.1 Sv and from 0 to 0.25 PW for the AX18 transect (Figs. 9c,d). This error probably arises from the smoothing of eddy features along the transect, particularly near the boundaries, as previously reported (Goes et al. 2015), but may be also sensitive to the method of mapping applied. The Argo estimated RMSE for the North Atlantic MOC and MHT show different changes with respect to spatial mapping. At the highest mapping resolution ($\Delta R = 0.25°$), the RMSE for Argo estimates are approximately 7.0 Sv and 0.65 PW relative

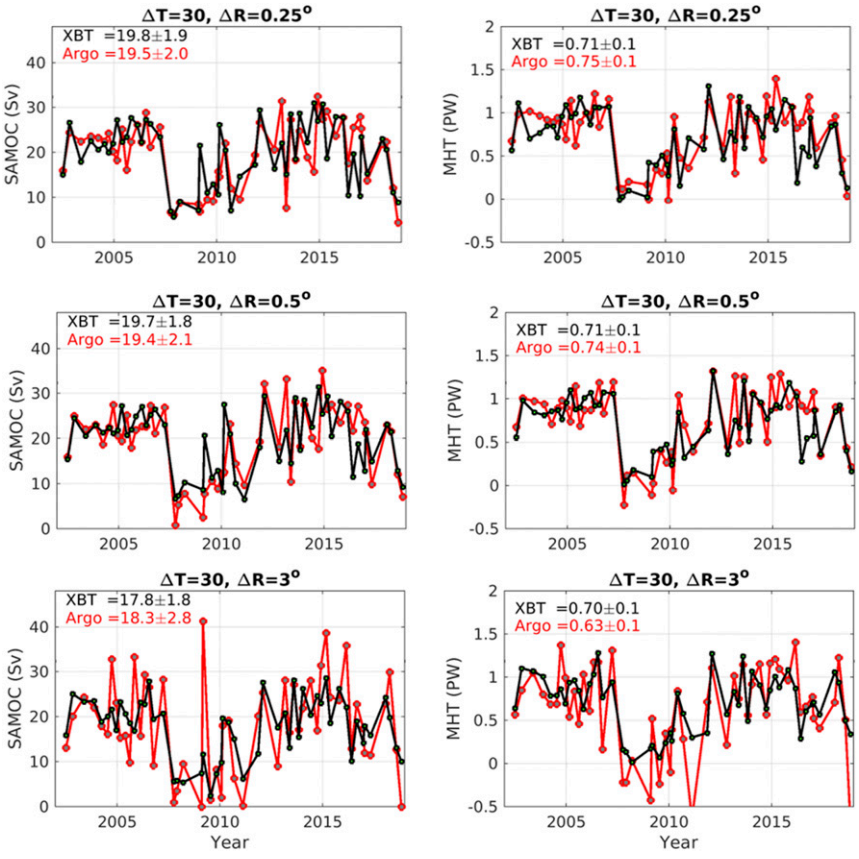

FIG. 8. Time series of the (left) South Atlantic MOC and (right) MHT estimated along the AX18 transect (see Fig. 1a) for Argo (red) and XBT (black) data for a ΔT = 30-day time mapping and spatial mapping of ΔR for (top) 0.25°, (middle) 0.5°, and (bottom) 3°. The time mean and 95% CI are included in each panel.

to the XBT baseline. By increasing the smoothing area, the RMSE for Argo estimates are considerably reduced (Figs. 9a,b), and for $\Delta R = 5°$ they reach 4.1 Sv and 0.40 PW and approach the error values of the XBTs under the same mapping resolution. In agreement with the density of profiles per area shown in Fig. 3, these results indicate that Argo and XBT-derived values for the MOC and MHT become more similar at low spatial resolutions. However, at low resolution the errors due to the smoothing of mesoscale features are significant and account for at least 25% of the mean. In the South Atlantic, the RMSE derived from Argo estimates relative to the AX18 XBT transect baseline is 6.1 Sv and 0.58 PW for $\Delta R = 0.25°$, with relatively small changes for varying mapping resolutions. At $\Delta R = 5°$, the errors decrease to 4.1 Sv and 0.40 PW. These errors are sensitive to the use of climatology to fill gaps in the Argo estimates, particularly for the low ΔR values, and without it the error values can reach 16.0 Sv and 0.8 PW for the MOC and MHT at $\Delta R = 0.25°$ mapping, which are as large as the mean values of these estimates themselves.

e. *Integrating Argo and XBT data*

In the previous sections we compared XBT and Argo estimates using data from these platforms independently. Here, we explore their complementarity using as an example the estimates of MHT and MOC in the North Atlantic, thus comparing the estimates produced from XBT data against XBT + Argo data. For this, we used a strategy similar to the one described in section 3c, with the difference that here we estimated the quantities along the nominal AX07 transect at monthly averages, instead of following each XBT transect realization. The nominal XBT transect was calculated as the median of all transect realizations after interpolating all realizations to a fixed distance of 25 km between profiles. Therefore, both Argo and XBT data samplings are subject to sparsity in the space and time dimensions. The sparsity of data can be visualized in a time × longitude diagram (Fig. 10), in which a matrix of markers shows the sampled locations along the nominal transect. XBT sampling started in 1995, closely following a quarterly temporal sampling. At 3° sampling, XBT data can produce a fairly even longitudinal coverage along the nominal AX07 transect despite some variability in the distance from each realization to its nominal transect. Due to ship route changes, there has been a slight shift in the AX07 transect location since 2010, resulting in larger gaps in the interior of the basin. The addition of Argo float data has a stronger impact in the sampling after 2002, and Argo data improve the sampling by closing the temporal and spatial gaps that are observed in the XBT data.

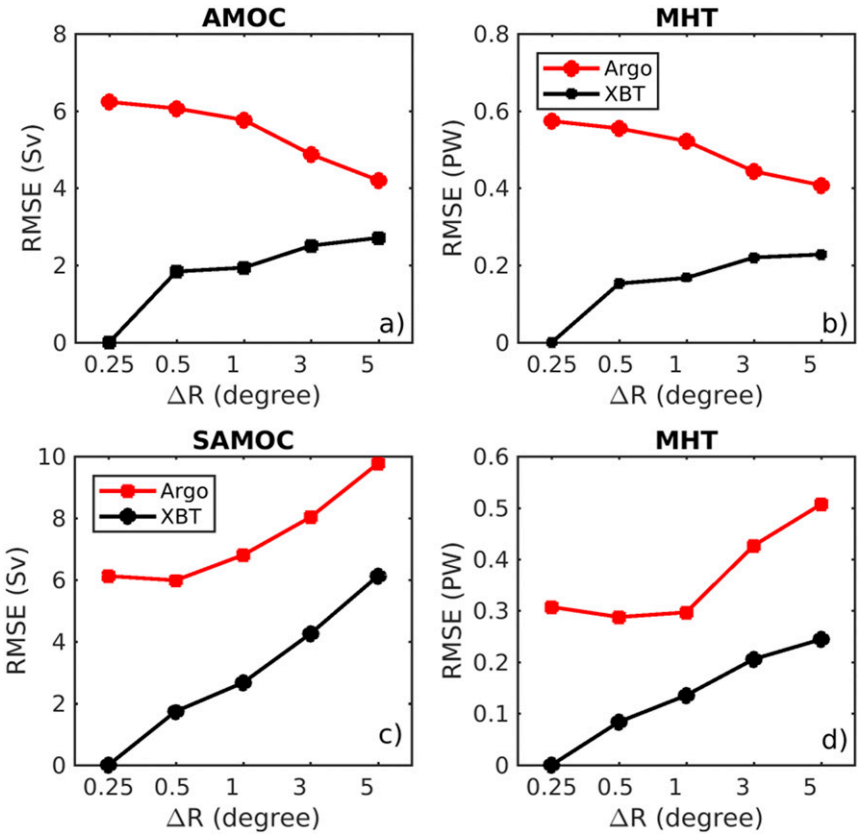

FIG. 9. Root-mean-square error (RMSE) of the (left) MOC and (right) MHT across the (a),(b) AX07 and (c),(d) AX18 transects as a function of ΔR using $\Delta T = 30$ days. The RMSE is calculated relative to the XBT baseline estimate with resolution of $\Delta R = 0.25°$ and $\Delta T = 30$ days.

The reconstructed monthly time series of MHT and MOC residuals using the combined Argo + XBT dataset is shown in Fig. 11, along with its comparison to the RAPIDMOCHA-WBTS monthly mean MOC estimates and the MHT estimates from Johns et al. (2011). The residuals are calculated by subtracting the mean values of the time series. The parameters selected for the comparison are $\Delta T = 30$ days and $\Delta R = 3°$, a compromise between resolution and coverage for both datasets. Although the location of the RAPID-MOCHA-WBTS array is different from the nominal AX07 transect, the combined Argo + XBT time series shows good agreement with the time series derived from RAPID-MOCHA-WBTS, producing a correlation of the monthly time series of 0.48 for both MOC and MHT (Figs. 11c,d). The correlations increase to 0.73 for MOC and 0.74 for MHT when only the months when XBT data are present in the combined Argo + XBT time series are accounted for, suggesting that the combination between XBT and Argo provides a better strategy to estimate the integrated meridional transports.

4. Discussion and conclusions

We analyzed the density of profiles from Argo floats along six XBT transects in the Atlantic Ocean, calculated their sampling trade-offs, and compared estimates of boundary current and basinwide meridional transports of volume and heat. By mapping the Argo and XBT data at different time scales and along-transect spatial resolution, we compared the sampling density between the two observational platforms. At higher-spatial-resolution mapping, such as 0.25° and 0.5°, Argo data density is too sparse, accounting for approximately 0.2 profiles per squared radius, which is less than that for XBTs by a factor of 10. The sampling trade-off between the two platforms shows that Argo sampling exceeds XBT sampling only in a small region for a wide range of resolutions considered, generally when resolutions are coarser than 3° and 30 days. However, at this sampling the boundary currents cannot be resolved, since they require a resolution better than 0.5° to resolve these narrow mesoscale features. Therefore, at higher spatial resolution, Argo cannot be used as a substitute for XBT sampling along boundary currents even for large temporal means.

We examined boundary currents in two regions, the Brazil Current at 22°S and the Gulf Stream near 37°N. At these locations, the low resolution optimal for Argo sampling may completely miss or even invert (in the case of the Brazil Current) the cross-current gradient. Thus, Argo float data cannot be used to measure currents on the shelf or on angled shelf breaks. This particularly affects the detection of features near or above the shelf, considerably reducing the

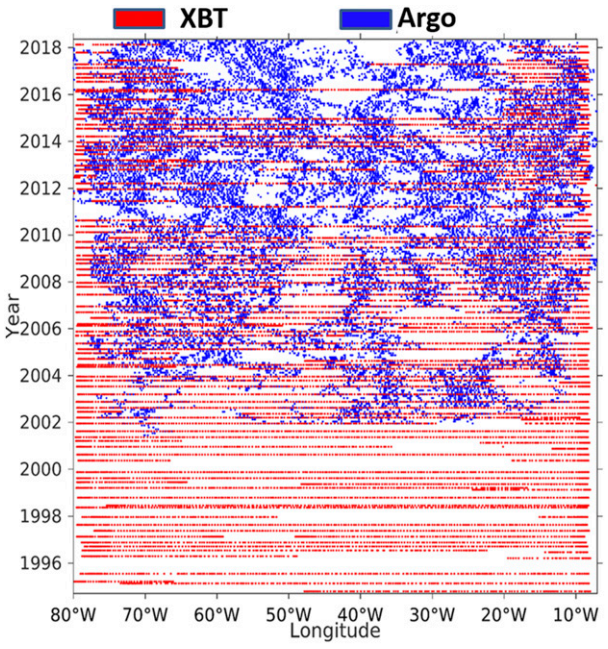

FIG. 10. Longitude–time diagram of the location of the sampled grid points along the nominal AX07 XBT transect using ΔT = 30 days and $\Delta R = 3°$ sampling for XBT (red) and Argo (blue) data.

ability to correctly attribute coastal sea level changes (e.g., Dong et al. 2019) and the impact of the ocean on regional air–sea interaction. Therefore, the current nominal XBT sampling resolution of 0.25° or higher near the boundaries provides better information than the Argo sampling in these regions.

With respect to cross-basin MHT and MOC, high spatial mapping resolution estimates from Argo produced a minimum RMSE of 0.3 PW and 6.0 Sv relative to the XBT baseline values, which represents approximately 30% of their long-term mean. At lower resolutions near 5° and 30-day mapping, Argo estimates in the North Atlantic converge to those from XBT estimates at the same resolution. However, at such a coarse resolution, the MOC and MHT errors have a lower limit of 3.0 Sv and 0.25 PW reached by the coarse resolution XBT transect relative to its baseline that resolves mesoscale features, and these values are also dependent on how the gaps are filled by climatological values.

In summary, XBTs provide sufficient spatial sampling to identify and resolve mesoscale features for currents and for MHT and MOC monitoring. Although Argo data do not provide a similar spatiotemporal sampling to XBT observations for the XBT transect regions, they are critical for determining reference velocity, large-scale salinity fields, and broadscale, basinwide features such as ocean gyres, ocean heat content, and steric sea level. The complementarity of these two observational platforms—that is, XBTs constraining along-transect mesoscale features and Argo constraining large-scale features—supports the joint use of both platforms to reduce temporal and spatial gaps in the global ocean observing system. We show that combining Argo and XBT observations along the nominal AX07 transect in the North Atlantic Ocean improves upper-ocean sampling, leading to a more effective identification of ocean currents, as well as large and mesoscale features needed to reduce uncertainties in the estimates of MHT and MOC along cross-basin transects.

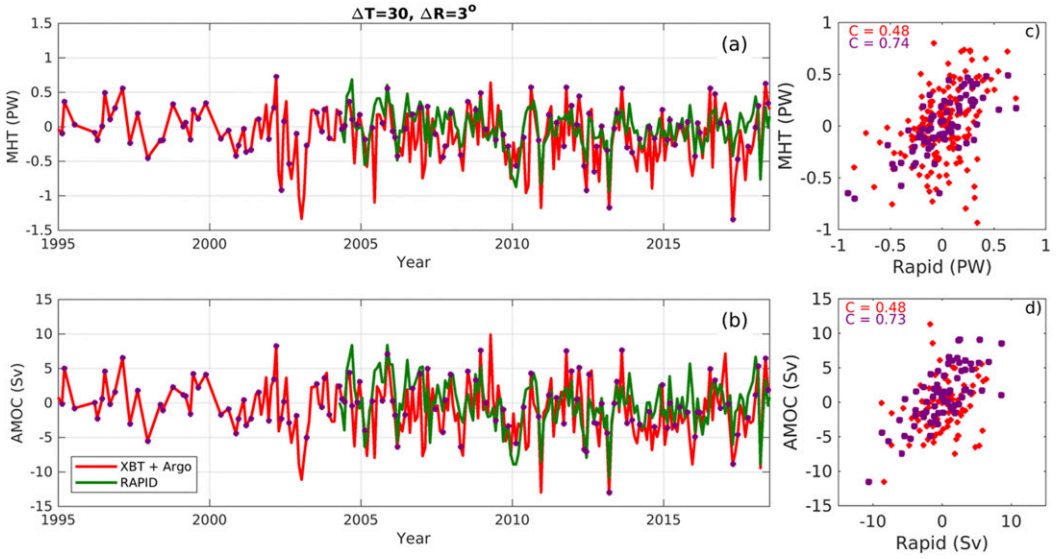

FIG. 11. Monthly residuals of (a) MHT and (b) Atlantic MOC strength along the nominal AX07 transect calculated from XBT + Argo (red) and RAPID data (green) using ΔT = 30 days and $\Delta R = 3°$ sampling. The residuals are calculated by subtracting the mean from all of the time series. The purple dots show the XBT + Argo estimates when data from the XBT transect are present. Also shown are scatterplots of (c) MHT and (d) AMOC for the XBT + Argo estimates (y axis) against RAPID (x axis), with purple dots for the XBT + Argo estimates when data from the XBT transect are present. The values of correlation are included on the top left of the panels.

Similar results should be expected for the MOC and MHT estimates in the South Atlantic. Combining XBTs and Argo measurements can also improve temporal and/or spatial sampling on BCS monitoring to detect frontal systems in the ACC, where the AX25 transect runs mostly during summer months.

Recent studies call for an integrated, multiplatform observing system to couple physical and biochemical variables for boundary currents and basin-integrated meridional transports (e.g., Stammer et al. 2019; Todd et al. 2019), which include Argo, XBTs, and other established and emerging platforms such as satellite altimetry and autonomous underwater vehicles. The unique value of the core Argo and XBT measurements consolidate these platforms as integral and necessary parts of the current global observing system to monitor surface, subsurface, and cross-basin transports. In other target areas, future studies could potentially apply a cost–benefit analysis to identify the observing platforms best suited to address current gaps in the observing system.

Acknowledgments. The authors thank Claudia Schmid and Chris Meinen for insights and comments on the paper. This research was accomplished under the auspices of the Cooperative Institute for Marine and Atmospheric Studies (CIMAS), a cooperative institute of the University of Miami and the National Oceanic and Atmospheric Administration (NOAA), Cooperative Agreement NA20OAR4320472, and was supported by the Ocean Observing and Monitoring Division of the NOAA Climate Program Office and by NOAA's Atlantic Oceanographic and Meteorological Laboratory (AOML) and the National Center For Environmental Information (NCEI).

Data availability statement. Data used for this study can be downloaded from the following URLs: Florida Current time series (http://www.aoml.noaa.gov/phod/floridacurrent/), XBT transect data (http://www.aoml.noaa.gov/phod/hdenxbt/), Argo profile data (https://www.nodc.noaa.gov/argo/ and http://doi.org/10.17882/42182), Argo climatological drifting velocity and ADT (http://apdrc.soest.hawaii.edu/projects/argo/), and the RAPID-MOCHA-WBTS MOC and MHT time series (https://www.rapid.ac.uk/rapidmoc/ and https://mocha.rsmas.miami.edu/mocha/).

REFERENCES

Andres, M., 2016: On the recent destabilization of the Gulf Stream path downstream of Cape Hatteras. *Geophys. Res. Lett.*, **43**, 9836–9842, https://doi.org/10.1002/2016GL069966.

Baehr, J., J. Hirschi, J.-O. Beismann, and J. Marotzke, 2004: Monitoring the meridional overturning circulation in the North Atlantic: A model-based array design study. *J. Mar. Res.*, **62**, 283–312, https://doi.org/10.1357/0022240041446191.

Boebel, O., R. E. Davis, M. Ollitraut, R. Peterson, P. Richard, C. Schmid, and W. Zenk, 1999: The intermediate depth circulation of the western South Atlantic. *Geophys. Res. Lett.*, **26**, 3329–3332, https://doi.org/10.1029/1999GL002355.

Boyer, T., and Coauthors, 2016: Sensitivity of global upper-ocean heat content estimates to mapping methods, XBT bias corrections, and baseline climatologies. *J. Climate*, **29**, 4817–4842, https://doi.org/10.1175/JCLI-D-15-0801.1.

Bryden, H., H. Longworth, and S. Cunningham, 2005: Slowing of the Atlantic meridional overturning circulation at 25°N. *Nature*, **438**, 655–657, https://doi.org/10.1038/nature04385.

Cheng, L., J. Zhu, R. Cowley, T. Boyer, and S. Wijffels, 2014: Time, probe type and temperature variable bias corrections to historical expendable bathythermograph observations. *J. Atmos. Oceanic Technol.*, **31**, 1793–1825, https://doi.org/10.1175/JTECH-D-13-00197.1.

——, and Coauthors, 2016: XBT science: Assessment of instrumental biases and errors. *Bull. Amer. Meteor. Soc.*, **97**, 924–933, https://doi.org/10.1175/BAMS-D-15-00031.1.

——, K. E. Trenberth, J. Fasullo, T. Boyer, J. Abraham, and J. Zhu, 2017: Improved estimates of ocean heat content from 1960 to 2015. *Sci. Adv.*, **3**, e1601545, https://doi.org/10.1126/sciadv.1601545.

da Silveira, I. C. A., L. Calado, B. M. Castro, M. Cirano, J. A. M. Lima, and A. S. Mascarenhas, 2004: On the baroclinic structure of the Brazil Current–intermediate western boundary current system at 22°–23°S. *Geophys. Res. Lett.*, **31**, L14308, https://doi.org/10.1029/2004GL020036.

Dee, D. P., and Coauthors, 2011: The ERA-Interim reanalysis: Configuration and performance of the data assimilation system. *Quart. J. Roy. Meteor. Soc.*, **137**, 553–597, https://doi.org/10.1002/qj.828.

Dieng, H. B., A. Cazenave, B. Meyssignac, and M. Ablain, 2017: New estimate of the current rate of sea level rise from a sea level budget approach. *Geophys. Res. Lett.*, **44**, 3744–3751, https://doi.org/10.1002/2017GL073308.

Domingues, R., G. Goni, S. Swart, and S. Dong, 2014: Wind forced variability of the Antarctic circumpolar current south of Africa between 1993 and 2010. *J. Geophys. Res.*, **119**, 1123–1145, https://doi.org/10.1002/2013JC008908.

——, ——, M. Baringer, and D. Volkov, 2018: What caused the accelerated sea level changes along the U.S. East Coast during 2010–2015? *Geophys. Res. Lett.*, **45**, 13 367–13 376, https://doi.org/10.1029/2018GL081183.

Dong, S., S. L. Garzoli, M. O. Baringer, C. S. Meinen, and G. J. Goni, 2009: Interannual variations in the Atlantic meridional overturning circulation and its relationship with the net northward heat transport in the South Atlantic. *Geophys. Res. Lett.*, **36**, L20606, https://doi.org/10.1029/2009GL039356.

——, M. Baringer, G. Goni, and S. Garzoli, 2011: Importance of the assimilation of Argo float measurements on the meridional overturning circulation in the South Atlantic. *Geophys. Res. Lett.*, **38**, L18603, https://doi.org/10.1029/2011GL048982.

——, G. Goni, and F. Bringas, 2015: Temporal variability of the South Atlantic meridional overturning circulation between 20°S and 35°S. *Geophys. Res. Lett.*, **42**, 7655–7662, https://doi.org/10.1002/2015GL065603.

——, M. Baringer, and G. Goni, 2019: Slow down of the Gulf Stream during 1993-2016. *Sci. Rep.*, **9**, 6672, https://doi.org/10.1038/s41598-019-42820-8.

Douglass, E., D. Roemmich, and D. Stammer, 2010: Interannual variability in North Pacific heat and freshwater budgets. *Deep-Sea Res. II*, **57**, 1127–1140, https://doi.org/10.1016/j.dsr2.2010.01.001.

Flagg, C. N., M. Dunn, D.-P. Wang, H. T. Rossby, and R. L. Benway, 2006: A study of the currents of the outer shelf and upper slope from a decade of shipboard ADCP observations in the Middle Atlantic Bight. *J. Geophys. Res.*, **111**, C06003, https://doi.org/10.1029/2005JC003116.

Fujii, Y., and Coauthors, 2019: Observing system evaluation based on ocean data assimilation and prediction systems: On-going challenges and a future vision for designing and supporting ocean observational networks. *Front. Mar. Sci.*, **6**, 417, https://doi.org/10.3389/fmars.2019.00417.

Goes, M., N. M. Urban, R. Tonkonojenkov, M. Haran, A. Schmittner, and K. Keller, 2010: What is the skill of ocean tracers in reducing uncertainties about ocean diapycnal mixing and projections of the Atlantic meridional overturning circulation? *J. Geophys. Res.*, **115**, C12006, https://doi.org/10.1029/2010JC006407.

——, G. Goni, V. Hormann, and R. C. Perez, 2013: Variability of the Atlantic off-equatorial eastward currents during 1993–2010 using a synthetic method. *J. Geophys. Res.*, **118**, 3026–3045, https://doi.org/10.1002/jgrc.20186.

——, ——, and S. Dong, 2015: An optimal XBT-based monitoring system for the South Atlantic meridional overturning circulation at 34°S. *J. Geophys. Res.*, **120**, 161–181, https://doi.org/10.1002/2014JC010202.

——, J. Christophersen, S. Dong, G. Goni, and M. O. Baringer, 2018: An updated estimate of salinity for the Atlantic Ocean sector using temperature–salinity relationships. *J. Atmos. Oceanic Technol.*, **35**, 1771–1784, https://doi.org/10.1175/JTECH-D-18-0029.1.

——, M. Cirano, M. M. Mata, and S. Majumder, 2019: Long-term monitoring of the Brazil Current transport at 22°S from XBT and altimetry data: Seasonal, interannual, and extreme variability. *J. Geophys. Res.*, **124**, 3645–3663, https://doi.org/10.1029/2018JC014809.

Goni, G. J., and M. O. Baringer, 2002: Surface currents in the tropical Atlantic across high density XBT line AX08. *Geophys. Res. Lett.*, **29**, 2218, https://doi.org/10.1029/2002GL015873.

——, and Coauthors, 2010: The Ship of Opportunity Program. *Proc. OceanObs'09*, Venice, Italy, European Space Agency, WPP-306, https://doi.org/10.5270/OceanObs09.cwp.35.

——, and Coauthors, 2019: More than 50 years of successful continuous temperature section measurements by the global expendable bathythermograph network, its integrability, societal benefits, and future. *Front. Mar. Sci.*, **6**, 452, https://doi.org/10.3389/fmars.2019.00452.

Johns, W. E., and Coauthors, 2011: Continuous, array-based estimates of Atlantic Ocean heat transport at 26.5°N. *J. Climate*, **24**, 2429–2449, https://doi.org/10.1175/2010JCLI3997.1.

Lebedev, K. V., H. Yoshinari, N. A. Maximenko, and P. W. Hacker, 2007: YoMaHa'07: Velocity data assessed from trajectories of Argo floats at parking level and at the sea surface. IPRC Tech. Note 4 (2), 20 pp., http://apdrc.soest.hawaii.edu/projects/Argo/data/Documentation/YoMaHa070612.pdf.

Locarnini, R. A., and Coauthors, 2013: *Temperature*. Vol. 1, *World Ocean Atlas 2013*, NOAA Atlas NESDIS 73, 40 pp., http://data.nodc.noaa.gov/woa/WOA13/DOC/woa13_vol1.pdf.

Lopez, H., S. Dong, S. Lee, and G. Goni, 2016: Decadal modulations of interhemispheric global atmospheric circulations and monsoons by the South Atlantic meridional overturning circulation. *J. Climate*, **29**, 1831–1851, https://doi.org/10.1175/JCLI-D-15-0491.1.

Lyman, J. M., J. K. Willis, and G. C. Johnson, 2006: Recent cooling in the upper ocean. *Geophys. Res. Lett.*, **33**, L18604, https://doi.org/10.1029/2006GL027033.

Majumder, S., M. Goes, P. S. Polito, R. Lumpkin, C. Schmid, and H. Lopez, 2019: Propagating modes of variability and their impact on the western boundary current in the South Atlantic. *J. Geophys. Res.*, **124**, 3168–3185, https://doi.org/10.1029/2018JC014812.

McCarthy, G. D., and Coauthors, 2015: Measuring the Atlantic meridional overturning circulation at 26°N. *Prog. Oceanogr.*, **130**, 91–111, https://doi.org/10.1016/j.pocean.2014.10.006.

Ridgway, K., R. Coleman, R. Bailey, and P. Sutton, 2008: Decadal variability of East Australian Current transport inferred from repeated high-density XBT transects, a CTD survey and satellite altimetry. *J. Geophys. Res.*, **113**, C08039, https://doi.org/10.1029/2007JC004664.

Riser, S., and Coauthors, 2016: Fifteen years of ocean observations with the global Argo array. *Nat. Climate Change*, **6**, 145–153, https://doi.org/10.1038/nclimate2872.

Rykova, T., and P. R. Oke, 2015: Recent freshening of the East Australian Current and its eddies. *Geophys. Res. Lett.*, **42**, 9369–9378, https://doi.org/10.1002/2015GL066050.

Stammer, D., and Coauthors, 2019: Ocean climate observing requirements in support of climate research and climate information. *Front. Mar. Sci.*, **6**, 444, https://doi.org/10.3389/fmars.2019.00444.

Sutton, R. T., and M. R. Allen, 1997: Decadal predictability of North Atlantic sea surface temperature and climate. *Nature*, **388**, 563–567, https://doi.org/10.1038/41523.

Swart, S., S. Speich, I. J. Ansorge, G. J. Goni, S. Gladyshev, and J. R. E. Lutjeharms, 2008: Transport and variability of the Antarctic Circumpolar Current south of Africa. *J. Geophys. Res.*, **113**, C09014, https://doi.org/10.1029/2007JC004223.

Todd, R. E., and Coauthors, 2019: Global perspectives on observing ocean boundary current systems. *Front. Mar. Sci.*, **6**, 423, https://doi.org/10.3389/fmars.2019.00423.

Vecchi, G. A., and M. J. Harrison, 2007: An observing system simulation experiment for the Indian Ocean. *J. Climate*, **20**, 3300–3319, https://doi.org/10.1175/JCLI4147.1.

Vidard, A., D. L. Anderson, and M. Balmaseda, 2007: Impact of ocean observation systems on ocean analysis and seasonal forecasts. *Mon. Wea. Rev.*, **135**, 409–429, https://doi.org/10.1175/MWR3310.1.

Visbeck, M., E. P. Chassignet, R. G. Curry, T. L. Delworth, R. R. Dickson, and G. Krahmann, 2003: The ocean's response to North Atlantic Oscillation variability. *The North Atlantic Oscillation: Climatic Significance and Environmental Impact*, *Geophys. Monogr.*, Vol. 134, Amer. Geophys. Union, 113–145.

Volkov, D. L., S.-K. Lee, R. Domingues, H. Zhang, and M. Goes, 2019: Interannual sea level variability along the southeastern seaboard of the United States in relation to the gyre-scale heat divergence in the North Atlantic. *Geophys. Res. Lett.*, **46**, 7481–7490, https://doi.org/10.1029/2019GL083596.

Wijffels, S., and G. Meyers, 2004: An intersection of oceanic waveguides: Variability in the Indonesian Throughflow region. *J. Phys. Oceanogr.*, **34**, 1232–1253, https://doi.org/10.1175/1520-0485(2004)034<1232:AIOOWV>2.0.CO;2.

Woodworth, P. L., M. Á. M. Maqueda, V. M. Roussenov, R. G. Williams, and C. W. Hughes, 2014: Mean sea-level variability along the northeast American Atlantic coast and the roles of the wind and the overturning circulation. *J. Geophys. Res. Oceans*, **119**, 8916–8935, https://doi.org/10.1002/2014JC010520.

Yu, P., S. L. Morey, and J. J. O'Brien, 2006: Development of new techniques for assimilating satellite altimetry data into ocean models. FSU Center for Ocean–Atmosphere Prediction Studies Paper, 2 pp., https://www.coaps.fsu.edu/~morey/GoM/08_Yu_Peng_WGNE_2006.pdf.

Zilberman, N. V., D. H. Roemmich, S. T. Gille, and J. Gilson, 2018: Estimating the velocity and transport of western boundary current systems: A case study of the East Australian Current near Brisbane. *J. Atmos. Oceanic Technol.*, **35**, 1313–1329, https://doi.org/10.1175/JTECH-D-17-0153.1.

Zuo, H., M. A. Balmaseda, S. Tietsche, K. Mogensen, and M. Mayer, 2019: The ECMWF operational ensemble reanalysis–analysis system for ocean and sea ice: A description of the system and assessment. *Ocean Sci.*, **15**, 779–808, https://doi.org/10.5194/os-15-779-2019.

Zweng, M. M., and Coauthors, 2013: *Salinity*. Vol. 2, *World Ocean Atlas 2013*, NOAA Atlas NESDIS 74, 39 pp., http://data.nodc.noaa.gov/woa/WOA13/DOC/woa13_vol2.pdf.